Quantitative comparison of amplitude and phase thermal responses on steels and ceramics through active thermography techniques

Proceedings IRF2020: 7th International Conference Integrity-Reliability-Failure.
J.F. Silva Gomes and S.A. Meguid (editors), INEGI-FEUP (2020), pp.197-206.
https://paginas.fe.up.pt/~irf/Proceedings_IRF2020/

PAPER REF: 17286

QUANTITATIVE COMPARISON OF AMPLITUDE AND PHASE THERMAL RESPONSES ON STEELS AND CERAMICS THROUGH ACTIVE THERMOGRAPHY TECHNIQUES

Raffaella Sesana[1(*)], Irene Pessolano Filos[1], Francesca Curà[1], Manuela De Maddis[2], Sebastiano Rizzo[3], Luca Corsaro[1]

[1]DIMEAS, Politecnico di Torino, Italy
[2]DIGEP, Politecnico di Torino, Italy
[3]Central Lab - Product Development, Tsubaki Nakashima, Italy
[(*)]*Email:* raffaella.sesana@polito.it

ABSTRACT

Active thermography NDT are full field, non contact techniques used on steel, composites and ceramics for defect and damage detection. In this paper, thermal parameters and material responses of samples are investigated quantitatively by means of theoretical and experimental approaches. Free material response to thermal loading is investigated for two classes of materials for structural applications: steel and ceramic.

Keywords: lock-in thermography, NDT, DFT analysis, thermal analysis, material characterization, train waves, steels, ceramics.

INTRODUCTION

There is considerable interest in active thermography techniques for Mechanical and Aerospace applications. Defects identification has become a central issue in structural studies and, as a result, much research in recent years has focused on the development of non-destructive techniques. Traditionally, systems are investigated by mechanical vibrations analysis. Researchers have studied and improved many aspects of material properties knowledge and response to thermal behavior. Recent studies on NDT focused on thermographic analysis. This technique is classified in two categories: Active (AT) and Passive (PT). The first differs from the latest for the excitation source. In passive thermography the thermal map is generally due to mechanical or physical phenomena occurring on the specimens, while in active thermography a thermal load, generally local and impulsive, is provided. Initial attempts focused on classifying active thermography techniques according to the excitation mechanism and the heating source. In structural industries and applications, the optical excitation mechanism is the most used. Metal defect detection and material characterization is performed with mainly two techniques known as Pulsed thermography (PT) [1]–[3] and Lock-in thermography (LT) [4]-[7]. These studies suggested possible experimental procedures for different active thermography techniques. Early data were interpreted by amplitude and phase images. An alternative approach was developed by [8][9]. In these studies, mathematical models were found to correlate sample temperature trends, material features and defects dimensions. [10] suggested a possible correlation function to relate whether a noisy thermal contrast evolution corresponds to a defect. [11] focused on identifying the reliability of thermography processing techniques by the use of the signal to noise ratio. Much research in recent years has explored the AT area. Previous works focused only on improvement of defect

detection sensibility. However, although the qualitative investigation to amplitude and phase images was demonstrated over the past years, little attention has been paid to the quantitative side. Few researchers have addressed the problem of a direct correlation between thermographic output and material characterization. A quantitative study can enable a deeper analysis of material characterization and defect identification.

In the present paper, in the mechanical and material field, a new approach is proposed: amplitude and phase of thermal response to a thermal impulse sequence are investigated in two different materials of structural interest. In particular, a set of steels and ceramics samples are excited by a laser impulse wave.

The purpose of this study is to quantitatively characterize the material behavior by means of active thermography; in particular, the main aim is defining an experimental procedure to point out the free thermal response parameters in the frequency domain which can lead to the follow up of microstructural damage phenomena in the investigated materials. The full material investigation covers also a Transient Analysis for the cooling down phase.

THEORETICAL BACKGROUND

AT implies an external excitation source. The specimen is therefore subject to heating up and cooling down phases. By means of an IR camera, both the temporal and spatial thermal evolution of the object are acquired. The output thermal imaging allows describing the heat pattern of an area or of a single pixel.

The transient temperature in a surface point, in result of a thermal impulse, is obtained by the Fourier law of heat conduction [11]:

$$\frac{\partial T}{\partial t} = \alpha \nabla^2 T \tag{1}$$

where $\alpha = \frac{k}{\rho c_p}$ [m^2/s] is the thermal diffusivity, k [W/mK] the thermal conductivity, ρ [kg/m^3] the density, c_p [J/kgK] the specific heat.

Assuming that the surface is uniformly heated, the 1D model brings to the thermal transient of a single point:

$$\frac{\partial T}{\partial t} = \alpha \frac{\partial^2 T}{\partial z^2} \tag{2}$$

Equation (2) is well known for the calculation of heat transfer across a conductive layer with a thermal gradient across the boundary surfaces. In case of an indefinite flat surface with thickness value neglectable with respect to the other dimensions, in adiabatic conditions, undergoing a it can be demonstrated that the time evolution of the average surface temperature is a thermal 1D process:

$$\iint_S T_{3D}(x, y, z = 0, t) dx dy = T_{1D}(z = 0, t) \tag{3}$$

Then, in case of semi-infinite homogenous, defect free material, the time-dependent surface temperature response to a periodic thermal wave with pulsation ω and wavelength λ, is calculated as the integral of the (2) that is [11]:

$$T_{(z,t)} = T_0 e^{\left(-\frac{z}{\mu}\right)} \cos\left(\frac{2\pi z}{\lambda} - \omega t\right) \tag{4}$$

T_0 is the initial temperature, $\omega=2\pi f$ [rad/s] is the modulated pulsation, f [Hz] is the modulated frequency, λ [m] is the thermal wavelength in the specimen. The diffusion length μ, that is a measure of the depth of a thermal wave with a given wavelength can probe within the sample is then [13]:

$$\mu = \sqrt{\frac{\alpha}{\pi f}} = \frac{\lambda}{2\pi} \tag{5}$$

If the specimen is thermally excited with a square wave, the excitation can be considered as the sum of sinusoidal harmonic contributions.

The DFT (Discrete Fourier Transformation) can give a description of the input signal energy content, in which the even terms are present [12]. The nth Amplitude DFT term follows the following equation [12]:

$$A_n = \frac{2}{\pi n} \tag{6}$$

By means of these pieces of information the energy contribution of each harmonic of the square wave can be calculated.

Then the cooling phase following a square wave excitation can be seen as the sum of the free responses to many harmonic excitations.

In the present paper the frequency-domain data processing is adopted to investigate the material behavior to free-response. Moreover, amplitude and phase spectra bring to system natural frequencies identification.

The shift from time to frequency domain is guaranteed by the Parseval's theorem: the energy associated with a signal must assume the same value in time and frequency:

$$\int_{-\infty}^{+\infty} (x(t))^2 dt = \int_{-\infty}^{+\infty} |X(f)|^2 df \tag{7}$$

Where $x(t)$ is the time signal function that admits the $X(f)$ transform function.

MATERIALS AND METHODS

Data obtained in previous studies [5], [9], [13]–[15] using active thermography techniques qualitatively compared amplitude and phase of thermal wave signals. In most cases, temperature profiles revealed considerable differences in thermal responses [10], [16]–[18]. According to He *et al.* (2013) raw thermal images gave the tool to detect inhomogeneities in materials. In the case of [19] pulsed thermography was useful to observe the thermal contrast of defects.

In the present paper, a methodology for material characterization by means of thermographic approach is proposed.

In the current investigation a total of 2 samples were analysed.

The investigated materials are standard steels as reported in [1, 5] and a ceramic material, in particular Silicon Nitride. In particular the first sample is a DP600 steel sheet 1,2mm thick, and the second sample is a Si_3N_4 ceramic disk 1,35 mm thick and 12,09 mm diameter.

For the selected materials, according to literature data [22][23], indicative values are reported in Table 1.

Table 1 - Materials physical properties

	k	c_P	ρ	α	μ
DP600	52	502	7850	1,3196E-05	14314,9
Si_3N_4	23	740	3260	9,5341E-06	7448,8

Steel sample was sprayed by means of a black opaque paint to improve emissivity. The Si_3N_4 specimen is gray and emissivity was measured in initial calibration phase.

The experimental set up is as shown in Figure 1.

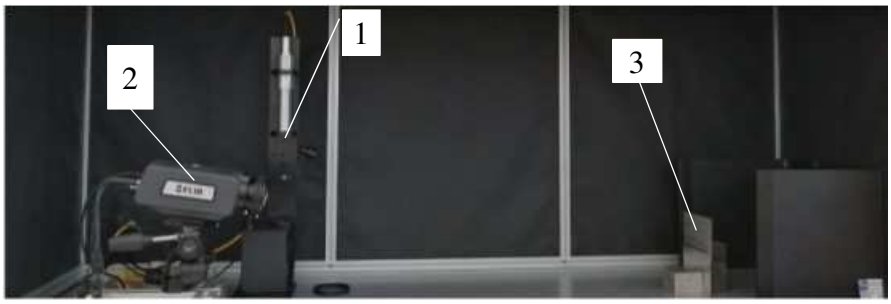

Fig. 1 - Experimental equipment: (1) laser source, (2) IR camera, (3) sample

The source of laser excitation is an IR waves generator, with a maximum power of 50 kW, triggered to provide a short output pulse to the sample. The IR camera thermal sensitivity is lower than 20 mK and operates in the 3-5 μm spectral range.

Laser excitation and IR camera acquisition parameters are selected after a sensitivity analysis, to maximize measuring performance and minimize acquisition errors.

Both laser and IR camera are controlled by a PC control unit in which a dedicated data processing software is installed.

The distance between the source and the sample is controlled. Environmental conditions, in particular, room temperature and humidity are monitored constantly for the test period by a thermometer and a hygrometer.

IR camera and laser parameters were selected using a revised version of pulsed and lock in thermography, reported by [24]. In particular, a sensitivity analysis was performed on laser power, number of impulses, pulse period, thermal load and acquisition path. The definitive experimental plan is reported in Table 2.

Table 2 - Experimental configurations

Test	Period [ms]	Laser %	Thermal energy [J]	Impulse number	Temperature window [°C]	Resolution window [pixels]	Frame Rate [Hz]
Test 1	50	40	100,00	1	10 - 90	160 x 128	785.67
Test 2	55	35	96,25	1	10 - 90	160 x 128	785.67
Test 3	60	30	90,00	1	10 - 90	160 x 128	785.67
Test 4	65	25	81,25	1	10 - 90	160 x 128	785.67
Test 5	70	20	70,00	1	10 - 90	160 x 128	785.67
Test 6	75	15	56,25	1	10 - 90	160 x 128	785.67
Test 7	80	11	44,00	1	10 - 90	160 x 128	785.67

Data processing refers to the time history of target pixel, that is the one with the maximum temperature measured during experiments.

The output thermal response was processed by means of the FFT and the frequency domain analysis on cooling phase temperature of the laser target point was performed. The numerical values of amplitude and phase were related to frequencies for the purpose of quantitative assessment.

The same cooling down phase was processed by means of a transient analysis processing routine. A Region of Interest (ROI) was identified on all samples and the transient analysis was conducted.

Amplitude, phase and thermal transients were compared for all materials: based on data obtained for 0,25 Hz and 10 Hz in the FFT plots, the parameters to measure the different behavior are defined as follows:

$$\Delta_{A\%} = \frac{A_{ceramic} - A_{steel}}{A_{intersection}} * 100 \tag{8}$$

$$\Delta_{\Phi\%} = \frac{\Phi_{ceramic} - \Phi_{steel}}{\Phi_{intersection}} * 100 \tag{9}$$

Furthermore, an analytical simulation was run to estimate the effect of the parameters in the thermal spectrum for the different materials. In particular a simplified model, taking into account for the different material physical properties was developed. In particular, the thermal amplitude spectrum was obtained considering in the integral (4) the contribution in amplitude.

RESULTS AND DISCUSSION

Processed results were quantitatively compared to study the thermal free response in the frequency domain. Using the data processing procedure above described, the free thermal response over frequency for steel and ceramic specimens were plotted.

In Figure 2 the plot of the FFT of the signal amplitude of the cooling phase is reported for the different testing configurations and the two materials, while in Figure 3 the corresponding plot of the FFT of the signal phase. Both diagrams are in log scales.

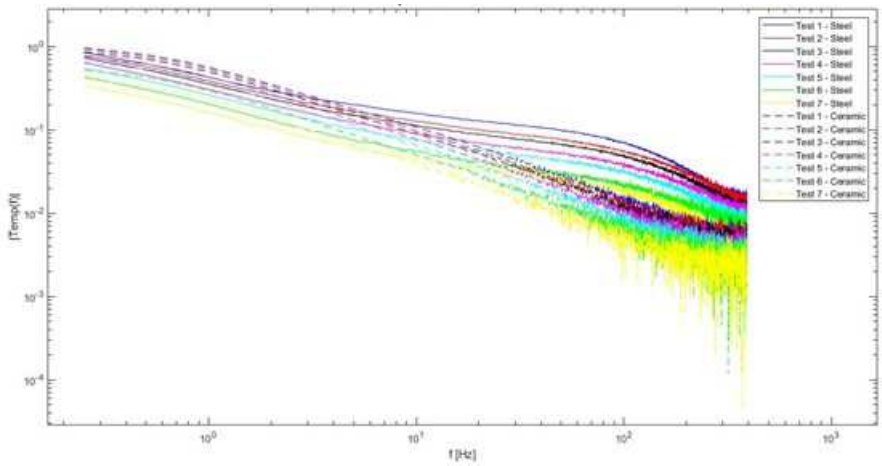

Fig. 2 - Steel and Ceramic thermal Amplitude over Frequency

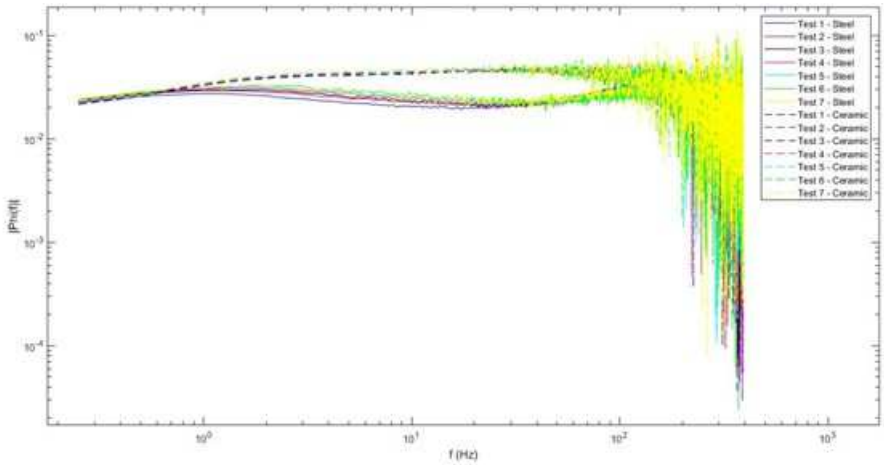

Fig. 3 - Steel and Ceramic thermal Phase over Frequency

It can be observed that, given the same testing conditions, ceramic and steel plots intersect. In Table 3 the intersection frequencies are reported for the amplitude (f_{IA}) and phase (f_{IF}) plots; in the same Table, the corresponding amplitude and phase values are reported for each testing configuration.

Table 3 - Amplitude and phase intersection frequencies and values

	f_{IA} **[Hz]**	**Amplitude**	f_{IF} **[Hz]**	**Phase**
Test 1	3,57	0,226	0,49	0,0256
Test 2	4,65	0,172	0,54	0,0260
Test 3	5,1	0,148	0,57	0,0278
Test 4	5,79	0,118	0,62	0,0290
Test 5	6,48	0,091	0,65	0,0296
Test 6	8,42	0,058	0,66	0,0298
Test 7	6,44	0,054	0,62	0,0298

In Table 2, column 4 it can be observed that from Test 1 to Test 7 configuration the amount of energy, supplyed to the specimen, decreases.

Given the input signal be a square wave, Figure 2 can be interpreted as the material response to a white energy spectrum: the amplitude plot gives the information about what are the "resonance" frequencies that is the frequencues to which the material is able to transmit the higher quantity of energy, while the phase plot indicates the frequencies in which the material dissipates or "elastically" reverse the energy incoming from the pulse.

In Figure 2 it can be observed that for every testing configuration, the energy associated to the corresponding frequency decreases with increasing frequency. The slope of this decrement is higher for the ceramic than for the steels. This can mean that the thermal stress produces higher amplitude response at low frequency for ceramics than for steels. This phenomenon occurs for every testing configuration.

In Figure 3 steel and ceramic show different behaviours. The spectrum highlights an almost flat behavior over the frequency range. Steel plots show two maximums for low and high frequencies, while ceramic plots a single maximum. These maximums can be interpreted according to Eq. (4). Given and instant *t* and a generic set coordinate *z*, the temperature related

to a defined wavelenght is given by the (4). Then the response of the materials for the different wavelength and then for the different frequencies, follows a sinusoidal trend, characterized then by maximums and minimums. The cycle period of ceramics appears then to be longer than the steel one.

In Table 3, comparing the values of amplitude and phase of the curves in the intersection points of ceramic and steel curves, it can be observed that amplitude values decrease from Tests 1 to 7 that is for impulse thermal energy decreasing. The phase values show an opposite behavior: decreasing the input energy, the phase in the intersection point increases. That is for lower energy higher dissipative phenomena take place.

To quantify and compare the difference between the thermal responses of the two materials, in Table 4 amplitude and phase % difference between the curves, according to (8) and (9) are reported. These parameters can give an estimation of the slope of the change of the response of the material thermal response with frequency. For low-frequency value f_{LOW}, the percentage change in amplitude is higher for tests with lower energy content, while an opposite behavior occurs at high-frequency f_{HIGH}: the percentage change in amplitude is lower for tests with lower energy content.

The same procedure is applied to determine phase changes. The phase variation for high frequency is one order of magnitude higher than for low frequency. This can mean that energy dissipation phenomena are different and more elevated for high frequency radiation for ceramic than for steel. This occurs for all testing configurations. It should be noticed that the phase starting values are considerably low and future works should deeply investigate the phenomenon.

Table 4 - Amplitude and phase % changes between ceramic and steel

Test	**f_{LOW}= 0,25 Hz**		**f_{HIGH}= 10 Hz**	
	Δ_A %	**Δ_Φ %**	**Δ_A %**	**Δ_Φ %**
Test 1	-50,71	2,58	21,65	-86,33
Test 2	-85,58	2,38	17,79	-80,85
Test 3	-89,59	2,23	16,19	-75,54
Test 4	-103,39	3,93	12,24	-69,52
Test 5	-115,38	3,78	9,49	-67,64
Test 6	-151,72	0,94	10,07	-66,78
Test 7	-126,67	3,83	10,37	-64,77

Furthermore, the difference in amplitude and phase spectrum for the two materials can be related to thermal and physical properties of the different materials.

In Table 5 the diffusion length for the two materials at 0,25 Hz and 10 Hz are calculated according to Table 1 physical properties.

Table 5 - Effusivity and diffusion length calculated data

	μ	$d_{0,25Hz}$	d_{10Hz}
DP600	14314,9	0,00410	0,00065
Si_3N_4	7448,8	0,00348	0,00055

The input thermal energy has a major effect on the specimen thickness. In low-frequency range, for ceramics, the reduced thermal conductivity compared to steel leads to higher amplitude values. These results of the experiments are in line with heat conduction law.

These plots confirm what is already known from physics: the different thermal conduction properties of ceramic and steel. Ceramic is considered to be thermally isolating while steel is considered thermally conductive. It can be pointed out that for the same energy supplied to steel and ceramic at low frequencies (Table 4, columns 2 and 3) steel shows a temperature lower than ceramic; the behaviour is opposite for higher frequencies (Table 4, columns 4 and 5). Lower frequencies have a higher penetration ability as shown in Table 5, and this effect is more evident for steel than for ceramic due to its isolating properties. The experimental confirmation comes from Figure 2 and Figure 3: given the same incoming spectrum, the ceramic excites mainly the lower frequencies, that is, it stores the incoming energy mainly at lower frequencies. The steel, which is a conductive material, shows a similar behaviour but the slope of amplitude vs frequency is lower, thus meaning that the received energy is distributed more uniformly on the frequency spectrum.

In Figure 4 the simulation of amplitude spectrum for steel specimen is reported in two testing conditions. The simulated curve approximates the trend and the values of the experimental ones thus showing that the thermal phenomena can be modelled as described as a thermal resonance response. The model requires further improvements.

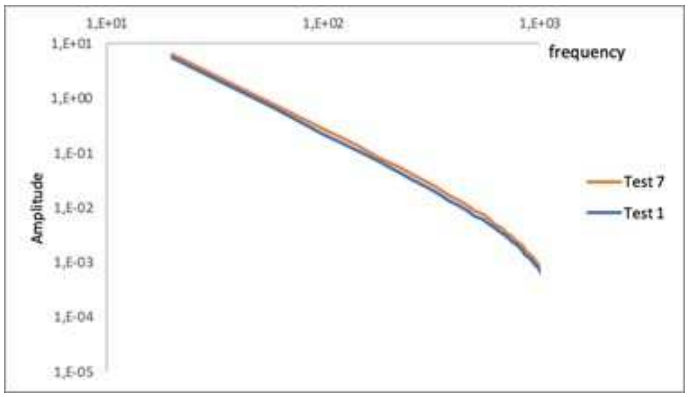

Fig. 4 - Simulated amplitude spectrum for DP600 specimen in different testing conditions

CONCLUSIONS

This research carries out non- destructive AT technique performance improving it and enhancing other possible fields.

In this study, different mechanical and structural materials, steel and ceramic, underwent thermal excitation with different energy content. Their thermal response is investigated by means of FFT analysis of the cooling transitory.

In addition, this study correlates the laser thermal energy with the intersection frequency of amplitude and phase. It was found that, for the same excitation thermal energy, steel and ceramics show different behaviour. FFT related parameters can be investigated to quantify these results.

REFERENCES

[1] He Y, Tian G, Pan M, Chen D, "Eddy current pulsed phase thermography and feature extraction," Appl. Phys. Lett., vol. 103, no. 8, p. 084104, Aug. 2013, doi: 10.1063/1.4819475.

[2] Larbi W. Ben, Klein M, Bendada A, Maldague X, "Experimental Comparison of Lock-in and Pulsed Thermography for the Nondestructive Evaluation of Aerospace Materials," Destr. Eval., no. June 2016, 2009.

[3] Huang R-S, Liu L-M, Song G, "Infrared temperature measurement and interference analysis of magnesium alloys in hybrid laser-TIG welding process," Mater. Sci. Eng. A, vol. 447, no. 1-2, pp.239-243, Feb. 2007, doi: 10.1016/j.msea.2006.10.069.

[4] Liu J, Yang W, Dai J, "Research on thermal wave processing of lock-in thermography based on analyzing image sequences for NDT," Infrared Phys. Technol., vol. 53, no. 5, pp.348-357, Sep. 2010, doi: 10.1016/j.infrared.2010.06.002.

[5] An Y-K, Kim J. Min, Sohn H, "Laser lock-in thermography for detection of surface-breaking fatigue cracks on uncoated steel structures," NDT E Int., vol. 65, pp.54-63, Jul. 2014, doi: 10.1016/j.ndteint.2014.03.004.

[6] Urbanek R, Bär J, "Evaluation of the Thermo-Elastic Behavior of a High-alloyed Steel by Fourier Transformation based Lock-In-Thermography," in Proceedings of the 2018 International Conference on Quantitative InfraRed Thermography, 2018, no. 3, pp.941-950, doi: 10.21611/qirt.2018.127.

[7] Bagavac P, "Lock-in thermography image procesing." p. 7.

[8] Halloua H, Obbadi A, Errami Y, Sahnoun S, Elhassnaoui A, "Nondestructive inverse approach for determining thermal and geometrical properties of internal defects in CFRP composites by lock-in thermography," Proc. 2016 Int. Conf. Electr. Sci. Technol. Maghreb, Cist. 2016, pp.1-7, 2017, doi: 10.1109/CISTEM.2016.8066828.

[9] Jinlong G, Junyan L, Fei W, Yang W, "Inverse heat transfer approach for nondestructive estimation the size and depth of subsurface defects of CFRP composite using lock-in thermography," Infrared Phys. Technol., vol. 71, pp.439-447, Jul. 2015, doi: 10.1016/j.infrared.2015.06.005.

[10] Xu C, Xie J, Huang W, Chen G, Gong X, "Improving defect visibility in square pulse thermography of metallic components using correlation analysis," Mech. Syst. Signal Process., vol. 103, pp.162-173, Mar. 2018, doi: 10.1016/j.ymssp.2017.09.030.

[11] Doshvarpassand S, Wu C, Wang X, "An overview of corrosion defect characterization using active infrared thermography," Infrared Phys. Technol., vol. 96, no. December 2018, pp.366-389, Jan. 2019, doi: 10.1016/j.infrared.2018.12.006.

[12] Bogatin E, Signal and Power Integrity - Simplified, 2nd Edition. Prentice Hall, 2009.

[13] Siddiqui JA, Arora V, Mulaveesala R, Muniyappa A, "Infrared Thermal Wave Imaging for Nondestructive Testing of Fibre Reinforced Polymers," Exp. Mech., vol. 55, no. 7, pp.1239-1245, Sep. 2015, doi: 10.1007/s11340-015-0019-z.

[14] Wu D, Busse G, "Lock-in thermography for nondestructive evaluation of materials," Rev. Générale Therm., vol. 37, no. 8, pp.693-703, Sep. 1998, doi: 10.1016/S0035-3159(98)80047-0.

[15] Holtmann N, Artzt K, Gleiter A, Strunk HP, Busse G, "Iterative improvement of Lockin-thermography results by temporal and spatial adaption of optical excitation," Quant. Infrared Thermogr. J., vol. 9, no. 2, pp.167-176, Dec. 2012, doi: 10.1080/17686733.2012.741919.

[16] Liu B, Zhang H, Fernandes H, Maldague X, "Experimental Evaluation of Pulsed Thermography, Lock-in Thermography and Vibrothermography on Foreign Object Defect (FOD) in CFRP," Sensors, vol. 16, no. 5, p. 743, May 2016, doi: 10.3390/s16050743.

[17] Yin A, Gao B, Tian G. Yun, Woo WL, Li K, "Physical interpretation and separation of eddy current pulsed thermography," J. Appl. Phys., vol. 113, no. 6, p. 064101, Feb. 2013, doi: 10.1063/1.4790866.

[18] Krankenhagen R, Ziegler M, "Systematic errors in the evaluation of uncorrected data from thermographic lock-in measurements," in Proceedings of the 2018 International Conference on Quantitative InfraRed Thermography, 2018, pp.539-547, doi: 10.21611/qirt.2018.054.

[19] Daryabor P, Safizadeh MS, "Comparison of three thermographic post processing methods for the assessment of a repaired aluminum plate with composite patch," Infrared Phys. Technol., vol. 79, pp.58-67, Nov. 2016, doi: 10.1016/j.infrared.2016.09.012.

[20] Toscano C, Riccio A, Camerlingo F, Meola C, "Lockin thermography to monitor propagation of delamination in CFRP composites during compression tests," in Proceedings of the 2012 International Conference on Quantitative InfraRed Thermography, 2012, doi: 10.21611/qirt.2012.335.

[21] Chatterjee K, Roy D, Tuli S, "A novel pulse compression algorithm for frequency modulated active thermography using band-pass filter," Infrared Phys. Technol., vol. 82, pp.75-84, May 2017, doi: 10.1016/j.infrared.2017.02.015.

[22] Den Uijl N, "Thermal and electrical resistance in resistance spot welding," no. May, 2008, doi: 10.13140/RG.2.1.3058.5204.

[23] Kitayama M, Hirao K, Toriyama M, Kanzaki S, "Thermal Conductivity of ß-Si3N4: I, Effects of Various Microstructural Factors," J. Am. Ceram. Soc., vol. 82, no. 11, pp.3105-3112, Dec. 2004, doi: 10.1111/j.1151-2916.1999.tb02209.x.

[24] Pitarresi G, Licari A, "Implementazione di tecniche di termografia attiva ir- ndt su compositi grp mediante la deposizione di impulsi termici di lunga durata," in Meccanica, 2011, pp.7-10.